

Excited State Dynamics of a Pt^{II} Diimine Complex bearing a Naphthalene-Diimide Electron Acceptor

Igor V. Sazanovich,[†] Mohammed A. H. Alamiry,[†] Jonathan Best,[†] Robert D. Bennett,[†] Oleg V. Bouganov,[‡] E. Stephen Davies,[§] Vyacheslav P. Grivin,^{||} Anthony J. H. M. Meijer,[†] Victor F. Plyusnin,^{||} Kate L. Ronayne,[⊥] Alexander H. Shelton,[†] Sergei A. Tikhomirov,[‡] Michael Towrie,[⊥] and Julia A. Weinstein^{*,†}

Department of Chemistry, University of Sheffield, Sheffield S3 7HF, United Kingdom, B.I. Stepanov Institute of Physics, Minsk, 220068, Belarus, School of Chemistry, University of Nottingham, Nottingham NG7 2RD, United Kingdom, Institute of Chemical Kinetics and Combustion, Novosibirsk, 630090, Russia, and Central Laser Facility, Science and Technology Facilities Council, Rutherford Appleton Laboratory, Harwell Science and Innovation Campus, Didcot, OX11 0QX, United Kingdom

Received June 3, 2008

A combination of picosecond time-resolved infrared spectroscopy, picosecond transient absorption spectroscopy, and nanosecond flash photolysis was used to elucidate the nature and dynamics of a manifold of the lowest excited states in Pt(phen-NDI)Cl₂ (**1**), where NDI = strongly electron accepting 1,4,5,8-naphthalene-diimide group. **1** is the first example of a Pt^{II}-diimine-diimide dyad. UV/vis/IR spectroelectrochemistry and EPR studies of electrochemically generated anions confirmed that the lowest unoccupied molecular orbital (LUMO) in this system is localized on the NDI acceptor group. The lowest allowed electronic transition in Pt(phen-NDI)Cl₂ is charge-transfer-to-diimine of a largely Pt→phen metal-to-ligand charge-transfer (MLCT) character. Excitation of **1** in the 355–395 nm range initiates a series of processes which involve excited states with the lifetimes of 0.9 ps (¹NDI*), 3 ps (³MLCT), 19 ps (vibrational cooling of “hot” ³NDI and of “hot” NDI ground state), and 520 μs (³NDI). Excitation of **1** with 395 nm femtosecond laser pulses populates independently the ¹MLCT and the ¹NDI* excited states. A thermodynamically possible decay of the initially populated ¹MLCT to the charge-transfer-to-NDI excited state, [Pt^{III}(phen-NDI⁻)Cl₂], is not observed. This finding could be explained by an ultrafast ISC of the ¹MLCT to the ³MLCT state which lies about 0.4 eV lower in energy than [Pt^{III}(phen-NDI⁻)Cl₂]. The predominant decay pathway of the ³MLCT is a back electron transfer process with ~3 ps lifetime, which also causes partial population of the vibrationally hot ground state of the NDI fragment. The decay of the ¹NDI* state in **1** populates vibrationally hot ground state of the NDI, as well as vibrationally hot ³NDI. The latter relaxes to form ³NDI state, that is, [Pt(phen-³NDI)Cl₂]*, which possesses a remarkably long lifetime for a Pt^{II} complex in fluid solution of 520 μs. The IR signature of this excited state includes the ν(CO) bands at 1607 and 1647 cm⁻¹, which are shifted considerably to lower energies if compared to their ground-state counterparts. The assignment of the vibrational bands is supported by the density-functional theory calculations in CH₂Cl₂. Pt(phen-NDI)Cl₂ acts as a modest photosensitizer of singlet oxygen.

Introduction

The presence of a manifold of close in energy excited states of different origin is a common feature of transition

metal complexes which determines their photophysical properties. Resolving the sequence of these excited states, as well as the rate and the pathways of the propagation of the excitation energy, is of particular fundamental interest and immediately relevant to the development of photoapplications. Transient electronic spectroscopy is the most common tool with which to follow the dynamics of the excited states. Yet, if multiple excited states are formed, electronic spectroscopy alone may not necessarily follow the

* To whom correspondence should be addressed. E-mail: julia.weinstein@sheffield.ac.uk.

[†] University of Sheffield.

[‡] B.I. Stepanov Institute of Physics.

[§] University of Nottingham.

^{||} Institute of Chemical Kinetics and Combustion.

[⊥] Rutherford Appleton Laboratory.

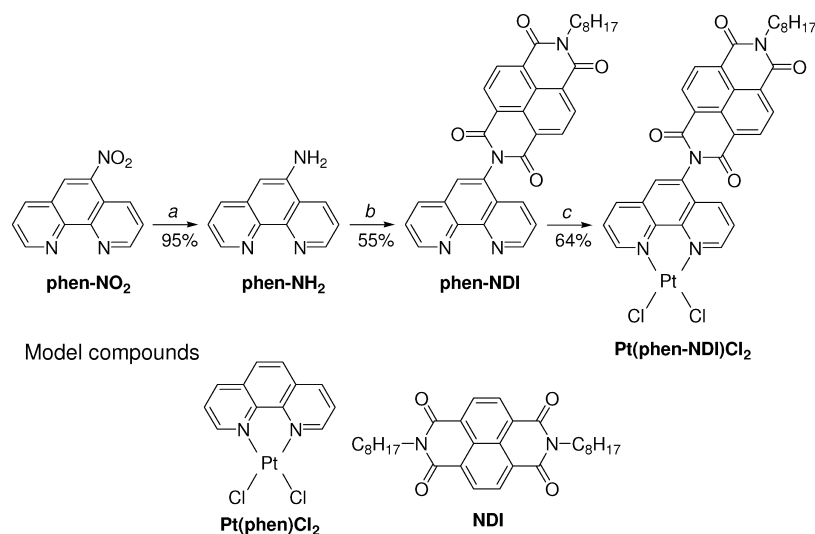
fate of each individual state. Time-resolved vibrational spectroscopy provides a powerful and complementary method to resolve a manifold of close-lying excited states as it probes molecular structure. Time-resolved vibrational spectroscopy is also invaluable for elucidating the dynamics of vibrationally hot electronic states which are frequently formed upon initial photoexcitation and play the key role in the ultrafast intramolecular energy redistribution.

A variety of photoapplications requiring strong absorption of visible light have utilized simple transition metal complexes and their assemblies with various organic chromophores. Aromatic acid imides are perhaps the most extensively used organic chromophores in this respect, largely because of their high photo- and chemical stability.¹ In a transition metal complex modified by an imide, a manifold of low-lying excited states may potentially include intraligand and intraimide excited states, metal-to-ligand charge-transfer (MLCT) states, and a charge-separated excited state in which the unpaired electron resides on the imide. For example, the long-lived triplet excited states of the imides have been explored in a range of biological applications.^{2–14} On the other hand, the strong electron accepting properties of the imides and the unique spectroscopic signature of each of the individual redox states^{15–18} led to their extensive use in photoinduced charge-separation assemblies for solar energy conversion.^{16,19–27} Imide substituted ligands have been successfully incorporated into

numerous metal complexes,^{28–35} including the d⁶-assemblies based on Ir(III)³⁶ and Ru^{II}.^{21,37–39} While these complexes are presently the major players in the field of photoinduced charge-separation, the Pt^{II}-based systems have been much less explored. Yet the initial introduction by Eisenberg of Pt^{II} contenders^{40–42} showed a significant promise of the square-planar d⁸ chromophores^{43–45} with respect to light-driven charge separation, their advantages comprising intense absorption of visible light, a lack of chirality, and directionality of electron transfer.

We report an insight into the photophysics of a simple Pt^{II}-diimine-imide model system, namely, Pt(phen-NDI)Cl₂, **1**, in which a Pt^{II} diimine unit (diimine = 1,10-phenanthroline, phen), is modified with a 1,4,5,8-naphthalene-diimide group, NDI. Once the photophysics of this simple unit is understood, it shall enable a diversity of modifications which could provide various charge-separation motifs or generate long-lived triplet excited states. We also take advantage of the useful feature of the imides which is surprisingly rarely explored^{46–48} —a

- (1) For a recent review please see: (a) Bhosale, S. V.; Jani, C. H.; Langford, S. J. *Chem. Soc. Rev.* **2008**, *37*, 331–342.
- (2) Aveline, B. M.; Matsugo, S.; Redmond, R. W. *J. Am. Chem. Soc.* **1997**, *119*, 11785–11795.
- (3) Green, S.; Fox, M. A. *J. Phys. Chem.* **1995**, *99*, 14752–14757.
- (4) McMasters, S.; Kelly, L. A. *J. Phys. Chem. B* **2006**, *110*, 1046–1055.
- (5) Abraham, B.; Kelly, L. A. *J. Phys. Chem. B* **2003**, *107*, 12534–12541.
- (6) Kawai, K.; Osakada, Y.; Fujitsuka, M.; Majima, T. *J. Phys. Chem. B* **2007**, *111*, 2322–2326.
- (7) Rogers, J. E.; Kelly, L. A. *J. Am. Chem. Soc.* **1999**, *121*, 3854–3861.
- (8) Rogers, J. E.; Le, T. P.; Kelly, L. A. *Photochem. Photobiol.* **2001**, *73*, 223–229.
- (9) Rogers, J. E.; Weiss, S. J.; Kelly, L. A. *J. Am. Chem. Soc.* **2000**, *122*, 427–436.
- (10) Ryan, G. J.; Quinn, S.; Gunnlaugsson, T. *Inorg. Chem.* **2008**, *47*, 401–403.
- (11) Vicić, D. A.; Odom, D. T.; Nunez, M. E.; Gianolio, D. A.; McLaughlin, L. W.; Barton, J. K. *J. Am. Chem. Soc.* **2000**, *122*, 8603–8611.
- (12) Weiss, S. J.; Rogers, J. E.; Kelly, L. A. *Photochem. Photobiol.* **1999**, *69*, 82S–83S.
- (13) Takenaka, S.; Uto, Y.; Saita, H.; Yokoyama, M.; Kondo, H.; Wilson, W. D. *Chem. Commun.* **1998**, 1111–1112.
- (14) Dixon, D. W.; Thornton, N. B.; Steullet, V.; Netzel, T. *Inorg. Chem.* **1999**, *38*, 5526–5534.
- (15) Andric, G.; Boas, J. F.; Bond, A. M.; Fallon, G. D.; Ghiggino, K. P.; Hogan, C. F.; Hutchison, J. A.; Lee, M. A. P.; Langford, S. J.; Pilbrow, J. R.; Troup, G. J.; Woodward, C. P. *Aust. J. Chem.* **2004**, *57*, 1011–1019.
- (16) Gosztoła, D.; Niemczyk, M. P.; Svec, W.; Lukas, A. S.; Wasielewski, M. R. *J. Phys. Chem. A* **2000**, *104*, 6545–6551.
- (17) Kolosov, D.; Adamovich, V.; Djurovich, P.; Thompson, M. E.; Adachi, C. *J. Am. Chem. Soc.* **2002**, *124*, 9945–9954.
- (18) Leedy, D. W.; Muck, D. L. *J. Am. Chem. Soc.* **1971**, *93*, 4264–4270.
- (19) Balan, B.; Gopidas, K. R. *Chem.—Eur. J.* **2007**, *13*, 5173–5185.
- (20) Addicott, C.; Oesterling, I.; Yamamoto, T.; Mullen, K.; Stang, P. J. *J. Org. Chem.* **2005**, *70*, 797–801.
- (21) Borgstrom, M.; Shaikh, N.; Johansson, O.; Anderlund, M. F.; Styring, S.; Akermark, B.; Magnuson, A.; Hammarstrom, L. *J. Am. Chem. Soc.* **2005**, *127*, 17504–17515.
- (22) Chernick, E. T.; Mi, Q. X.; Vega, A. M.; Lockard, J. V.; Ratner, M. A.; Wasielewski, M. R. *J. Phys. Chem. B* **2007**, *111*, 6728–6737.
- (23) Flamigni, L.; Ventura, B.; You, C. C.; Hippus, C.; Wurthner, F. *J. Phys. Chem. C* **2007**, *111*, 622–630.
- (24) Greenfield, S. R.; Svec, W. A.; Gosztoła, D.; Wasielewski, M. R. *J. Am. Chem. Soc.* **1996**, *118*, 6767–6777.
- (25) Nakano, A.; Osuka, A.; Yamazaki, T.; Nishimura, Y.; Akimoto, S.; Yamazaki, I.; Itaya, A.; Murakami, M.; Miyasaka, H. *Chem.—Eur. J.* **2001**, *7*, 3134–3151.
- (26) Prodi, A.; Chiorboli, C.; Scandola, F.; Ingó, E.; Alessio, E. *ChemPhysChem* **2006**, *7*, 1514–1519.
- (27) Rachford, A. A.; Goeb, S.; Castellano, F. N. *J. Am. Chem. Soc.* **2008**, *130*, 2766–2767.
- (28) McAdam, C. J.; Manning, A. R.; Robinson, B. H.; Simpson, J. *Inorg. Chim. Acta* **2005**, *358*, 1673–1682.
- (29) Hodgkiss, J. M.; Damrauer, N. H.; Presse, S.; Rosenthal, J.; Nocera, D. G. *J. Phys. Chem. B* **2006**, *110*, 18853–18858.
- (30) Kelley, R. F.; Shin, W. S.; Rybtchinski, B.; Sinks, L. E.; Wasielewski, M. R. *J. Am. Chem. Soc.* **2007**, *129*, 3173–3181.
- (31) Kirmaier, C.; Hindin, E.; Schwartz, J. K.; Sazanovich, I. V.; Diers, J. R.; Muthukumar, K.; Taniguchi, M.; Bocian, D. F.; Lindsey, J. S.; Holten, D. *J. Phys. Chem. B* **2003**, *107*, 3443–3454.
- (32) Redmore, N. P.; Rubtsov, I. V.; Therien, M. J. *J. Am. Chem. Soc.* **2003**, *125*, 8769–8778.
- (33) Saito, K.; Kashiwagi, Y.; Ohkubo, K.; Fukuzumi, S. *J. Porphyrins Phthalocyanines* **2006**, *10*, 1371–1379.
- (34) Shavaleev, N. M.; Adams, H.; Best, J.; Weinstein, J. A. *J. Organomet. Chem.* **2007**, *692*, 921–925.
- (35) Shavaleev, N. M.; Davies, E. S.; Adams, H.; Best, J.; Weinstein, J. A. *Inorg. Chem.* **2008**, *47*, 1532–1547.
- (36) Flamigni, L.; Baranoff, E.; Collin, J. P.; Sauvage, J. P. *Chem.—Eur. J.* **2006**, *12*, 6592–6606.
- (37) Hossain, M. D.; Haga, M.; Gholamkhash, B.; Nozaki, K.; Tsumihama, M.; Ikeda, N.; Ohno, T. *Collect. Czech. Chem. Commun.* **2001**, *66*, 307–337.
- (38) Johansson, O.; Borgstrom, M.; Lomoth, R.; Palmblad, M.; Bergquist, J.; Hammarstrom, L.; Sun, L. C.; Akermark, B. *Inorg. Chem.* **2003**, *42*, 2908–2918.
- (39) Tyson, D. S.; Luman, C. R.; Zhou, X. L.; Castellano, F. N. *Inorg. Chem.* **2001**, *40*, 4063–4071.
- (40) McGarrath, J. E.; Kim, Y. J.; Hissler, M.; Eisenberg, R. *Inorg. Chem.* **2001**, *40*, 4510–4511.
- (41) Chakraborty, S.; Wadas, T. J.; Hester, H.; Schmehl, R.; Eisenberg, R. *Inorg. Chem.* **2005**, *44*, 6865–6878.
- (42) Chakraborty, S.; Wadas, T. J.; Hester, H.; Flaschenreim, C.; Schmehl, R.; Eisenberg, R. *Inorg. Chem.* **2005**, *44*, 6284–6293.
- (43) Sautter, A.; Kaletas, B. K.; Schmid, D. G.; Dobrawa, R.; Zimine, M.; Jung, G.; van Stokkum, I. H. M.; De Cola, L.; Williams, R. M.; Wurthner, F. *J. Am. Chem. Soc.* **2005**, *127*, 6719–6729.
- (44) Danilov, E. O.; Pomestchenko, I. E.; Kinayyigit, S.; Gentili, P. L.; Hissler, M.; Ziesel, R.; Castellano, F. N. *J. Phys. Chem. A* **2005**, *109*, 2465–2471.
- (45) Monnereau, C.; Gomez, J.; Blart, E.; Odobel, F. *Inorg. Chem.* **2005**, *44*, 4806–4817.

Scheme 1. Synthesis of the New Ligand Phen-NDI and the Pt(phen-NDI)Cl₂ (**1**) Complex, and Structures of the Model Compounds^a

^a Reaction conditions: (a) hydrazine hydrate (excess), Pd/C (catalyst), ethanol, N₂, reflux, 24 hr; (b) *N*-octyl-1,4,5,8-naphthalenetetracarboxylic monoanhydride, dry DMF, N₂, reflux, 24 hr; (c) Pt(DMSO)₂Cl₂, ethanol, N₂, reflux, 24 hr.

presence of the strongly IR active $\nu(\text{CO})$ and $\nu(\text{CC})$ vibrations, which enables the use of time-resolved infrared spectroscopy⁴⁹ to follow excited-state dynamics.

The present work combines picosecond and nanosecond transient absorption spectroscopy with picosecond time-resolved infrared spectroscopy to resolve excited-state dynamics in **1**, including an identification of the IR spectroscopic signature of NDI triplet excited state, and an investigation of the role of vibrationally hot electronic states in the process of redistribution of excitation energy.

Results

Synthesis and Characterization. The synthesis of the new ligand, phen-NDI, was achieved in two steps (Scheme 1). In the first step, 5-nitro-1,10-phenanthroline was reduced to 5-amino-1,10-phenanthroline (phen-NH₂) in quantitative yield using hydrazine hydrate as a reducing agent in the presence of Pd/C as a catalyst.⁵⁰ In the second step, phen-NH₂ was reacted with *N*-octyl-1,4,5,8-naphthalenetetracarboxylic monoanhydride³⁵ at reflux in DMF to provide phen-NDI in 65% yield. The ligand was purified by column chromatography on silica. The corresponding Pt(phen-NDI)Cl₂ complex was prepared by a reaction of Pt(DMSO)₂Cl₂⁵¹ with phen-NDI in ethanol at reflux and was sufficiently soluble in CH₂Cl₂ to be purified by column chromatography on silica. Both the ligand and the Pt^{II}

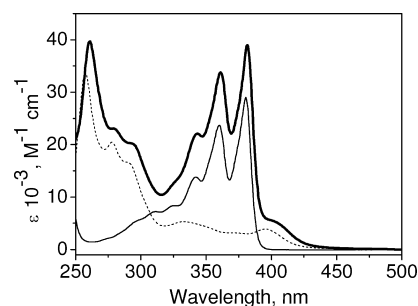


Figure 1. Ground state electronic absorption spectra of Pt(phen-NDI)Cl₂ (thick solid line), NDI (thin solid line) and Pt(phen)Cl₂ (dashed line), in CH₂Cl₂ at r.t.

complex were characterized by elemental analysis and ¹H NMR spectroscopy.

Electronic Absorption Spectra. The ground-state UV/vis absorption spectra of **1** (thick line), NDI (thin solid line), and Pt(phen)Cl₂ (thin dashed line) are depicted in Figure 1. The absorption spectrum of NDI is dominated by a transition to the lowest excited singlet S₁ state of NDI^{7,52–54} in the range 320–390 nm with the well-resolved vibronic structure. The spectrum of Pt(phen)Cl₂ contains an intense intraphenanthroline absorption at about 260 nm, and an MLCT absorption band at 395 nm. More stringently, the lowest absorption band at 395 nm should be assigned as a {charge-transfer-to-diimine} transition, as it has been shown that the Cl ligand makes a contribution into the highest occupied molecular orbital (HOMO). However, since the “MLCT” assignment is used routinely for Pt(diimine)Cl₂, this abbreviation is kept throughout the paper.

The absorption spectrum of **1** is merely a superposition of the unperturbed absorption bands of NDI and Pt(phen)Cl₂.

(46) Rubtsov, I. V.; Kang, Y. K.; Redmore, N. P.; Allen, R. M.; Zheng, J. R.; Beratan, D. N.; Therien, M. J. *J. Am. Chem. Soc.* **2004**, *126*, 5022–5023.

(47) Rubtsov, I. V.; Redmore, N. P.; Hochstrasser, R. M.; Therien, M. J. *J. Am. Chem. Soc.* **2004**, *126*, 2684–2685.

(48) Polyansky, D. E.; Danilov, E. O.; Castellano, F. N. *Inorg. Chem.* **2006**, *45*, 2370–2372.

(49) Butler, J. M.; George, M. W.; Schoonover, J. R.; Dattelbaum, D. M.; Meyer, T. J. *Coord. Chem. Rev.* **2007**, *251*, 492–514.

(50) Gunnlaugsson, T.; Leonard, J. P.; Senechal, K.; Harte, A. J. *J. Am. Chem. Soc.* **2003**, *125*, 12062.

(51) Price, J. H.; Williamson, A. N.; Schramm, R. F.; Wayland, B. B. *Inorg. Chem.* **1972**, *11*, 1280.

(52) Demeter, A.; Berces, T.; Biczok, L.; Wintgens, V.; Valat, P.; Kossanyi, J. *J. Phys. Chem.* **1996**, *100*, 2001–2011.

(53) Le, T. P.; Rogers, J. E.; Kelly, L. A. *J. Phys. Chem. A* **2000**, *104*, 6778–6785.

(54) Posokhov, Y.; Alp, S.; Koz, B.; Dilgin, Y.; Icli, S. *Turkish J. Chem.* **2004**, *28*, 415–424.

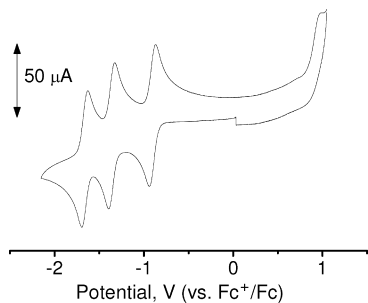


Figure 2. Cyclic voltammetry of 1 mM Pt(phen-NDI)Cl₂ in DMF containing 0.2 M [NBu₄][BF₄].

A shoulder at 395 nm ($\epsilon = 6.0 \times 10^3$ L/mol cm) was resolved by Gaussian deconvolution and attributed to a Pt \rightarrow phen MLCT transition. This observation indicates rather weak electronic interaction between NDI and Pt(phen)Cl₂ fragments in **1** in its ground state. This finding is not surprising as orientation of the plane of the imide group of NDI relative to the attached aromatic N-substituent is normally found to be nearly orthogonal,^{52,55} imposing weak if any electronic interaction. The orthogonality of the phen- and NDI-planes has been proved by density-functional theory (DFT) calculations (see Supporting Information). Thus, the lowest detectable absorption band in the spectrum of **1** corresponds to a (Pt \rightarrow phen) transition because of a lack of the spatial overlap for HOMO–LUMO Pt \rightarrow NDI transitions. The assignment of the HOMO and the lowest unoccupied molecular orbital (LUMO) is provided in the following two parts.

Cyclic Voltammetry. Cyclic voltammetry of a solution of Pt(phen-NDI)Cl₂ in DMF containing 0.2 M (NBu₄)BF₄ shows a series of three reversible, one-electron reduction processes at $E_{1/2}$: -0.90, -1.36, and -1.66 V versus Fc⁺/Fc (Figure 2). The CV of Pt(phen-NDI)Cl₂ in CH₂Cl₂ is shown in the Supporting Information, Figure SI 1.

On the basis of these values, the first and second reduction processes are assigned to NDI.^{7,16,38} The third reduction process occurs at a potential very close to that of Pt(phen)Cl₂ (-1.61 V) and is assigned to the reduction of coordinated 1,10-phenanthroline (see below).

An oxidation peak, at E_p^a +0.97 V versus Fc⁺/Fc, was noted close to the solvent breakdown. A similar oxidation for Pt(phen)Cl₂ was observed but at significantly lower potential (E_p^a +0.82 V vs Fc⁺/Fc). This might suggest that the HOMO is largely localized on the Pt center as in the other Pt(diimine)Cl₂ complexes.

UV/vis Spectroelectrochemistry. The nature of the frontier orbitals and the chemical reversibility of the redox processes of **1** were investigated by UV/vis spectroelectrochemistry at 253 K in DMF. The spectra corresponding to the individual redox states are presented in Figure 3, and the absorption data are summarized in Table 1. All three reduction processes are chemically reversible under those conditions. The absorption spectra of mono- and dianions **1**¹⁻ and **1**²⁻ match those reported previously for NDI anion and dianion.^{15,16,35} The spectral profile of the product of the

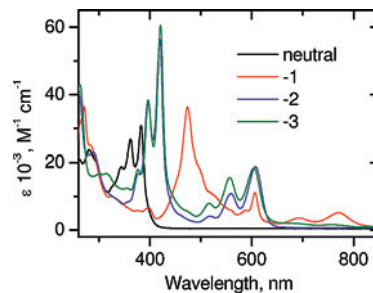


Figure 3. UV–vis spectra of neutral **1** (black line), **1**¹⁻ (red line), **1**²⁻ (blue line) and **1**³⁻ (green line) recorded at 253 K in DMF containing 0.2 M [NBu₄][BF₄].

Table 1. Absorption Spectra of the Neutral and Reduced Forms of Pt(phen-NDI)Cl₂, **1**, and Pt(phen)Cl₂ Complexes

complex	absorption data λ_{\max}/nm ($\epsilon \cdot 10^{-3}/\text{M}^{-1} \text{cm}^{-1}$)
	In CH ₂ Cl ₂ at r.t.
1 ⁰	261 (39.7), 343 (22.1), 361 (33.8), 382 (39.0)
	Obtained in spectroelectrochemical experiments in DMF/0.2 M [NBu ₄][BF ₄] ^a
1 ⁰	281 (23.7), 345 (18.7), 362 (26.9), 383 (30.9)
1 ¹⁻	324 (10.1), 375 (5.9), 398 (6.6), 474 (36.3), 588 (5.9), 606 (11.1), 693 (3.6), 770 (5.2)
1 ²⁻	289 (22.9), 377 (16.7), 396 (38.3), 420 (56.6), 519 (4.1), 559 (10.8), 607 (18.7)
1 ³⁻	301 (16.8), 314 (16.8), 354 (12.4), 376 (18.0), 397 (38.3), 421 (60.6), 516 (7.9), 557 (15.6), 604 (18.4), 762 (1.6), 859 (1.3)
Pt(phen)Cl ₂	279 (19.8), 369 (3.5), 391 (3.7)
Pt(phen)Cl ₂ ¹⁻	310 (10.2), 436 (3.0), 530 (1.7), 573 (2.5), 640 (1.9)

^a Data obtained at 253 K for Pt(phen-NDI)Cl₂ and 273 K for Pt(phen)Cl₂. The experimental error for extinction coefficient values obtained from spectroelectrochemical experiments is $\pm 500 \text{ M}^{-1} \text{cm}^{-1}$.

third one-electron reduction process is consistent with the superposition of the spectrum of the NDI²⁻ anion with that of the spectrum of coordinated phenanthroline-anion (Supporting Information, Figure SI 2, Table 1).

EPR Spectroscopy of Electrochemically Generated Mono, Di, and Trianions of Pt(phen-NDI)Cl₂ in DMF. EPR spectroscopic studies were carried out for the anionic species obtained by controlled potential electrolysis in DMF containing 0.2 M [NBu₄][BF₄]. Experimental and simulated EPR spectra are given in Figure 4.

The first one-electron reduction process produced a radical-monoanion [Pt(phen-NDI)Cl₂]¹⁻, the EPR spectrum of which, at 298 K, was characteristic of a NDI-based reduction.¹⁵ The experimental spectral profile was reproduced by the coupling of the unpaired electron to a combination of three pairs of hydrogen nuclei and one pair of nitrogen nuclei (Figure 4). The second reduction process yielded a spectrum essentially identical to that of the monoanion albeit with only 2.2% of the double integrated intensity; this fact indicated that electron spin pairing had taken place upon generation of the radical dianion, [Pt(phen-NDI)Cl₂]²⁻. Hence the second reduction process was also located on the NDI fragment, and the first and second reduction processes correspond to a consecutive population of the LUMO of the neutral species.

The EPR spectrum of the three-electron reduced product, **1**³⁻ (Figure 4 c,d) was recorded at 298 and 77 K. In fluid solution, a broad spectrum, centered at g_{iso} 1.981, was obtained and was consistent with an unpaired electron localized on a [Pt(phen)] moiety, although no Pt hyperfine splitting was resolved. At 77 K, the frozen solution spectrum

(55) Lukas, A. S.; Zhao, Y.; Miller, S. E.; Wasielewski, M. R. *J. Phys. Chem. B* **2002**, 1299–1306.

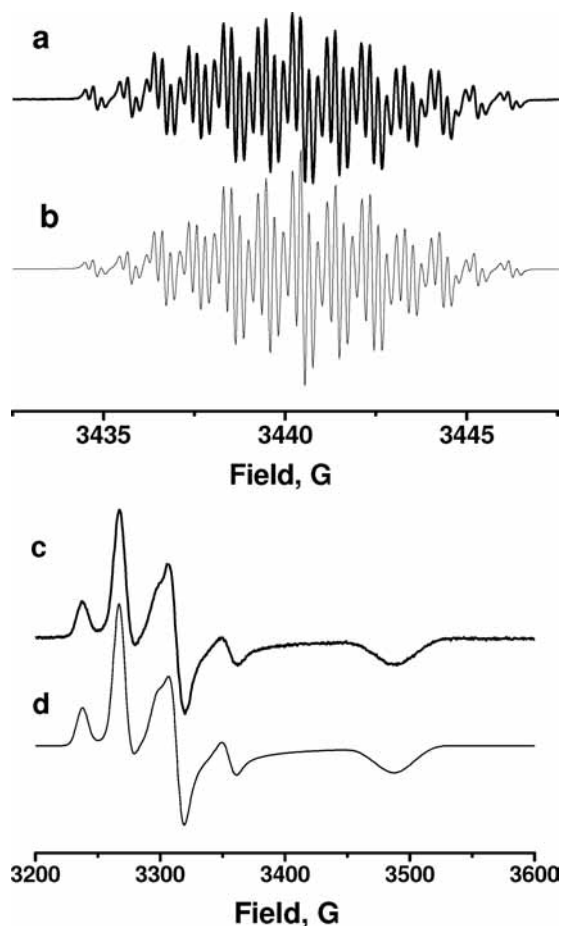


Figure 4. (a) Experimental EPR spectra of 1 mM $[\text{Pt}(\text{phen-NDI})\text{Cl}_2]^{-\bullet}$ in DMF containing 0.2 M $[\text{Bu}_4\text{N}][\text{BF}_4]$ at 298 K. (b) Simulation of the spectrum (a) using the following parameters: $g_{\text{iso}} = 2.004$, $a_{2\text{H}} 1.99 \times 10^{-4} \text{ cm}^{-1}$, $a_{2\text{H}} 1.58 \times 10^{-4} \text{ cm}^{-1}$, $a_{2\text{H}} 0.20 \times 10^{-4} \text{ cm}^{-1}$, $a_{2\text{N}} 0.89 \times 10^{-4} \text{ cm}^{-1}$. The spectra were simulated using Lorentzian line shape and 0.11 G line width. (c) Experimental EPR spectra of 1 mM $[\text{Pt}(\text{phen-NDI})\text{Cl}_2]^{3-}$ in DMF containing 0.2 M $[\text{Bu}_4\text{N}][\text{BF}_4]$ at 77 K. (d) Simulation of spectrum (c) using Gaussian line shape and the following parameters: $g_{xx} 2.001$, $A_{xx} -78.5 \times 10^{-4} \text{ cm}^{-1}$, $W_{xx} 9.5 \text{ G}$; $g_{yy} 2.030$, $A_{yy} -56.4 \times 10^{-4} \text{ cm}^{-1}$, $W_{yy} 9.0 \text{ G}$; $g_{zz} 1.902$, $A_{zz} -15.1 \times 10^{-4} \text{ cm}^{-1}$, $a_{2\text{N}} 8.9 \times 10^{-4} \text{ cm}^{-1}$, $W_{zz} 12 \text{ G}$.

was rhombic, with Pt hyperfine splitting distinguished clearly in g_{xx} and g_{yy} , with values of $A_{xx} -78.5 \times 10^{-4} \text{ cm}^{-1}$ and $A_{yy} -56.4 \times 10^{-4} \text{ cm}^{-1}$ obtained from simulation of the experimental spectrum. For g_{zz} , coupling was not observed directly, and the shape of this feature was best reproduced by a combination of metal ($A_{zz} -15.1 \times 10^{-4} \text{ cm}^{-1}$) and ligand ($a_{2\text{N}} 8.9 \times 10^{-4} \text{ cm}^{-1}$) components. This spectrum resembles that of other $[\text{Pt}(\text{diimine})\text{R}_2]^{-}$ based radical anions (R = Cl, thiolate, or catecholate/2), in which electron density is located largely at the diimine ligand, with some 7–13% contribution from the metal.^{35,56–59} The Pt contribution for $[\text{Pt}(\text{phen-NDI})\text{Cl}_2]^{3-}$ was estimated as about 13% following the same methodology.

- (56) McInnes, E. J. L.; Farley, R. D.; Macgregor, S. A.; Taylor, K. J.; Yellowlees, L. J.; Rowlands, C. C. *J. Chem. Soc., Faraday Trans.* **1998**, *94*, 2985–2991.
 (57) McInnes, E. J. L.; Farley, R. D.; Rowlands, C. C.; Welch, A. J.; Rovatti, L.; Yellowlees, L. J. *J. Chem. Soc., Dalton Trans.* **1999**, 4203–4208.
 (58) Adams, C. J.; Fey, N.; Weinstein, J. A. *Inorg. Chem.* **2006**, *45*, 6105–6107.
 (59) Weinstein, J. A.; Tierney, M. T.; Davies, E. S.; Base, K.; Robeiro, A. A.; Grinstaff, M. W. *Inorg. Chem.* **2006**, *45*, 4544–4555.

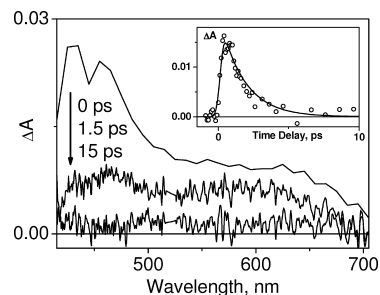


Figure 5. Transient absorption spectra of $\text{Pt}(\text{phen})\text{Cl}_2$ in CH_2Cl_2 , following excitation with 395 nm, 150 fs laser pulse. The spectrum at 0 time delay was reconstructed by a global fit analysis. The inset shows a decay trace averaged over the range 470–480 nm (O) and a fit to the data which comprises the deconvolved instrument response and a mono-exponential decay with the $1.7 \pm 0.5 \text{ ps}$ lifetime.

Picosecond Transient Absorption Data. Transient absorption experiments were performed on a solution of **1** in CH_2Cl_2 at room temperature in the spectral range from 410 to 725 nm. For comparison, $\text{Pt}(\text{phen})\text{Cl}_2$ was studied under identical conditions.

Excitation of $\text{Pt}(\text{phen})\text{Cl}_2$ with $\sim 150 \text{ fs}$, 395 nm laser pulse which coincides with the maximum of the $^1\text{MLCT}$ absorption, generates transient absorption bands with the maxima at 450 and 580 nm (Figure 5). These transient bands decay with the same lifetime of $1.7 \pm 0.5 \text{ ps}$ as obtained by a global fitting procedure. It has been reported previously that the rate of intersystem crossing (ISC) is about 230 fs in MLCT state of $\text{fac-}[\text{Re}(\text{stpy})(\text{CO})_3\text{bpy}]^{+60}$ and is quoted as $15 \pm 10 \text{ fs}$,⁶¹ 40 fs,⁶² or faster than 150 fs⁶³ in the MLCT state of Ru^{II} bipyridine complexes. Since the MLCT state of $\text{Pt}(\text{phen})\text{Cl}_2$ is formed in the immediate Pt^{II} coordination environment, it can be assumed that the rate of ISC in this complex is not significantly slower than that in Ru^{II} or Re^{I} diimine complexes. Consequently, the transient absorption spectrum recorded is assigned to the $^3\text{MLCT}$ excited state of $\text{Pt}(\text{phen})\text{Cl}_2$. The spectral dynamics faster than 1.7 ps similar to that reported for MLCT states in diimine complexes of Re^{I} ⁶⁴ and Ru^{II} ⁶⁵ was observed in the short wavelength region of the spectrum (410–450 nm) but could not be resolved because of the time resolution of the setup.

Excitation of **1** by $\sim 150 \text{ fs}$, 395 nm laser pulses results in a broad spectrum across the registration range (Figure 6). On the picosecond time scale, spectral evolution is wavelength dependent, indicating the presence of several excited states. The zero time delay spectrum (Figure 6a) was reconstructed by performing the global fitting procedure for the set of decay kinetics which were sliced across the spectral range. Each decay kinetics was constructed from the raw transient spectra by integrating over a 10 nm spectral

- (60) Busby, M.; Matousek, P.; Towrie, M.; Vlček, A. J. *J. Phys. Chem. A* **2005**, *109*, 3000–3008.
 (61) Cannizzo, A.; van Mourik, F.; Gawelda, W.; Zgrabcic, G.; Bressler, C.; Chergui, M. *Angew. Chem., Int. Ed.* **2006**, *45*, 3174–3176.
 (62) Bhasikuttan, A. C.; Suzuki, M.; Nakashima, S.; Okada, T. *J. Am. Chem. Soc.* **2002**, *124*, 8398–8405.
 (63) Yeh, A. T.; Shank, C. V.; McCusker, J. K. *Science* **2000**, *289*, 935–938.
 (64) Liard, D. J.; Busby, M.; Matousek, P.; Towrie, M.; Vlček, A. J. *Phys. Chem. A* **2004**, *108*, 2363–2369.
 (65) Wallin, S.; Davidsson, J.; Modin, J.; Hammarstrom, L. *J. Phys. Chem. A* **2005**, *109*, 4697–4704.

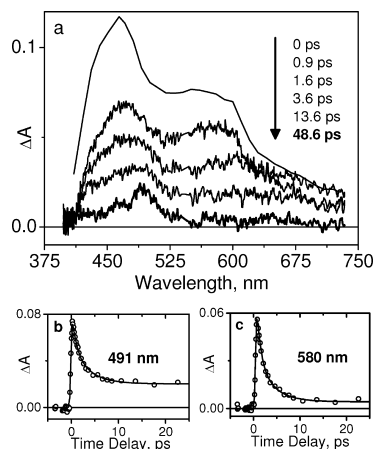


Figure 6. Transient absorption results obtained for Pt(phen-NDI)Cl₂ in CH₂Cl₂ following excitation with 395 nm, 150 fs laser pulse. (a). Transient absorption spectra at different time delays. The spectrum at 0 time delay was reconstructed by global fit analysis. (b) and (c): Transient absorption decay kinetics detected at 491 nm (b) and 580 nm (c). Each kinetic trace was fitted with a biexponential function with the lifetimes of $\tau_1 = 0.9 \pm 0.3$ ps and $\tau_2 = 3.5 \pm 1.1$ ps obtained by global fit, and a constant term (solid lines).

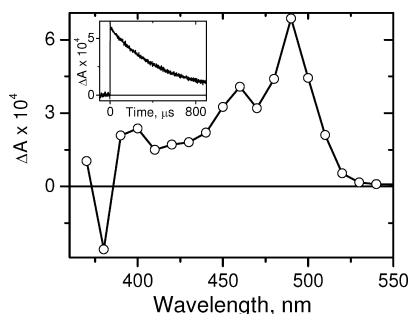


Figure 7. Transient absorption spectrum of Pt(phen-NDI)Cl₂ in CH₂Cl₂ at 50 ns time delay following excitation with 355 nm, 7 ns laser pulse. The inset shows a transient absorption decay trace measured at 490 nm along with the single-exponential fitting curve.

intervals. A minimum set of parameters which would allow for a consistent fit of the kinetic data included two mono-exponential decay processes along with one long-lived process which was modeled as a constant on a picosecond time scale. Accordingly, each kinetic trace was fitted with a biexponential decay and a constant term convolved with the instrument response function (Figure 6b,c). The lifetimes of the two decay processes obtained by global fitting are $\tau_1 = 0.9 \pm 0.3$ ps and $\tau_2 = 3.5 \pm 1.1$ ps. The spectral evolution ends by 50 ps (Figure 6), yielding a transient spectrum which is consistent with that obtained on the microsecond time scale by the flash photolysis method (Figure 7) and corresponds to the transient absorption spectrum of ³NDI excited state.^{2,3,7} The detailed discussion of the picosecond transient absorption results is given below.

Nanosecond Laser Flash Photolysis Data. The transient absorption spectra and kinetics obtained in flash photolysis experiments under ~ 7 ns, 355 nm excitation of a solution of **1** in CH₂Cl₂ are shown in Figure 7. The transient spectrum shows a bleach of the ground-state absorption at 380 nm and transient bands at 460 and 490 nm, which match precisely the spectrum of ³NDI.^{2,3,7} The transient spectrum decays simultaneously to the baseline with the 520 μ s lifetime.

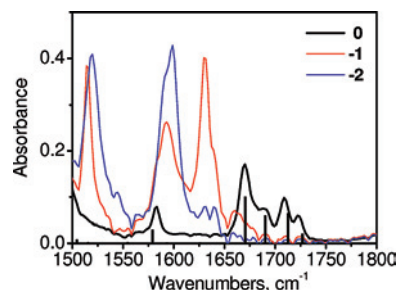


Figure 8. Infrared spectra of neutral **1** (black line), monoanion **1**⁻ (red line), and dianion **1**²⁻ (blue line) in CH₂Cl₂ containing 0.4 M [NBu₄][BF₄] at r.t. Vertical bars show IR frequencies calculated for ground singlet state of *N*-phenanthroline-*N'*-ethyl-naphthalene-diimide in CH₂Cl₂; the calculated frequencies are scaled by 0.98.

It should be noted that significant quenching of the ³NDI excited state has been observed at higher sample concentrations and excitation energies, presumably because of triplet-triplet annihilation^{7,9,66} which caused the transient spectrum to decay via mixed second and first order rate laws. To avoid the self-quenching, a set of photolysis experiments was performed with a gradually decreasing sample concentration and laser pulse energy until the decay trace could be fitted satisfactorily with the mono-exponential decay. This was achieved at 4×10^{-6} M concentrations, and yielded the lifetime of 520 ± 50 μ s quoted above. The observation of self-quenching is not surprising given the amenity of both Pt^{II} square planar systems⁶⁷⁻⁷⁰ and NDI-type molecules to aggregation^{2,21,71} and the long lifetime of the excited state. In the ground state, some deviation from Beer's law in the absorption spectra of **1** in CH₂Cl₂ was detected at and above 1×10^{-5} M concentration.

In acetonitrile, on the time scale of flash photolysis experiments the initial formation of the triplet state of **1** is followed by an intermolecular electron transfer which leads to the quenching of the triplet state and to the formation of the NDI-localized radical-anion, that is, [Pt(phen-NDI^{•-})Cl₂]. This behavior had been reported previously^{2,7,72} for the NDI-type systems and was not investigated further.

FTIR Spectra of Neutral and Reduced Species. The FTIR spectrum of **1** (thick line, Figure 8) in CH₂Cl₂ in the range from 1200 to 1800 cm⁻¹ is dominated by NDI vibrational bands, with no prominent vibrational bands of the phenanthroline being observed.

The main difference between the FTIR spectra of **1**, the uncoordinated phen-NDI ligand, and *N,N'*-dioctyl-NDI (Supporting Information, Figure SI 3) is that the $\nu(\text{CO})$ bands observed at 1666 cm⁻¹ and 1705 cm⁻¹ in the symmetric *N,N'*-

(66) Wintgens, V.; Valat, P.; Kossanyi, J.; Biczok, L.; Demeter, A.; Berces, T. *J. Chem. Soc., Faraday Trans.* **1994**, *90*, 411-421.

(67) Siemeling, U.; Bausch, K.; Fink, H.; Bruhn, C.; Baldus, M.; Angerstein, B.; Plessow, R.; Brockhinke, A. *Dalton Trans.* **2005**, 2365-2374.

(68) Houlding, V. H.; Miskowski, V. N. *Coord. Chem. Rev.* **1991**, *111*, 145.

(69) Yam, V. W.-W.; Wong, K. M.-C.; Zhu, N. *J. Am. Chem. Soc.* **2002**, *124*, 6506.

(70) Connick, W. B.; Henling, L. M.; Marsh, R. E.; Gray, H. B. *Inorg. Chem.* **1996**, *35*, 6261.

(71) Abraham, B.; McMasters, S.; Mullan, M. A.; Kelly, L. A. *J. Am. Chem. Soc.* **2004**, *126*, 4293-4300.

(72) Barros, T. C.; Brochsztain, S.; Toscano, V. G.; Berci, P.; Politi, M. J. *J. Photochem. Photobiol., A: Chem.* **1997**, *111*, 97-104.

Table 2. FTIR Data for Several Redox Forms of **1** in CH₂Cl₂ Containing 0.4 M [NBu₄][BF₄], and Picosecond TRIR Data in CH₂Cl₂^a

species	band position, cm ⁻¹
FTIR in the range 1500–1900 cm ⁻¹	
1 ⁰	1583, 1670, 1688 (sh), 1705, 1723 (sh)
1 ⁻	1514, 1592 (1583 sh), 1631, 1660
1 ²⁻	1519, 1599, 1629, 1639
TRIR in the range 1500–1680 cm ⁻¹	
	1576 (hot GS), 1599 (hot ³ NDI), 1607 (² NDI), 1647 (² NDI), 1660 (hot GS)

^a The assignment of the bands in the excited state is given in brackets.

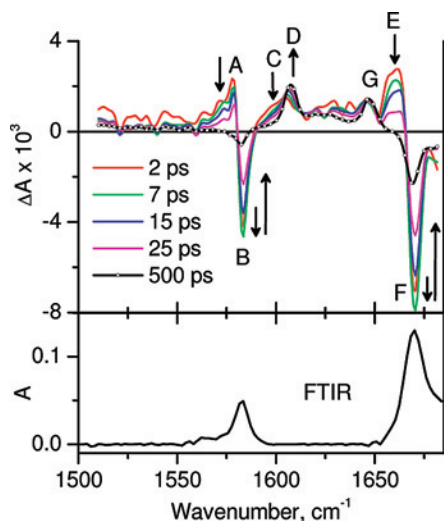


Figure 9. Upper panel: time-resolved infrared spectra of Pt(phen-NDI)Cl₂ in CH₂Cl₂ at different time delays following excitation with 395 nm, 150 fs laser pulse. Transient bands referred to in Figure 10 are labeled with letters A–G. Lower panel: ground-state FTIR spectrum of Pt(phen-NDI)Cl₂ in CH₂Cl₂ in the spectral range used in the TRIR experiments.

dioctyl-NDI are shifted to somewhat higher energies and split into two bands each, 1670 cm⁻¹ and 1688 cm⁻¹, and 1705 cm⁻¹ and 1723 cm⁻¹, respectively, upon covalent linkage to phen. This effect is clearly caused by an asymmetry of the NDI fragment in phen-NDI and in **1**. The band at 1583 cm⁻¹ which is not affected by the asymmetric substitution of the NDI group in **1** is also present in the IR spectrum of naphthalene and 1,8-naphthalic anhydride but not of glutarimide. DFT calculations performed on *N,N'*-ethyl-1,4,5,8-naphthalenediimide in CH₂Cl₂ (see below) suggest that this vibration is largely ν(CC) of the aromatic rings of the NDI, which is weakly coupled to the CH vibrations and to the vibrations of the carboxylic groups.

DFT calculations (Supporting Information) predict for the singlet state of *N,N'*-diethyl-NDI in CH₂Cl₂ the following frequencies (scaled by a standard factor of 0.98): 1708 and 1682 cm⁻¹, due to ν(CO), and 1581 cm⁻¹ due to ν(CC) of the aromatic rings of the NDI. These values match well the experimentally recorded frequencies at 1705, 1688, and 1583 cm⁻¹. The relatively low intensity of the phenanthroline-localized vibrations if compared to the NDI-localized ones is also supported by the DFT calculations.

The FTIR spectra of the monoanion **1**⁻ and bis-anion of **1**²⁻ (Figure 8, Table 2), which were generated from **1** in a CH₂Cl₂/[NBu₄][BF₄] (0.4 M) solution by control potential electrolysis, show a considerable shift of the ν(CO) bands to lower frequencies upon reduction, which reflects a

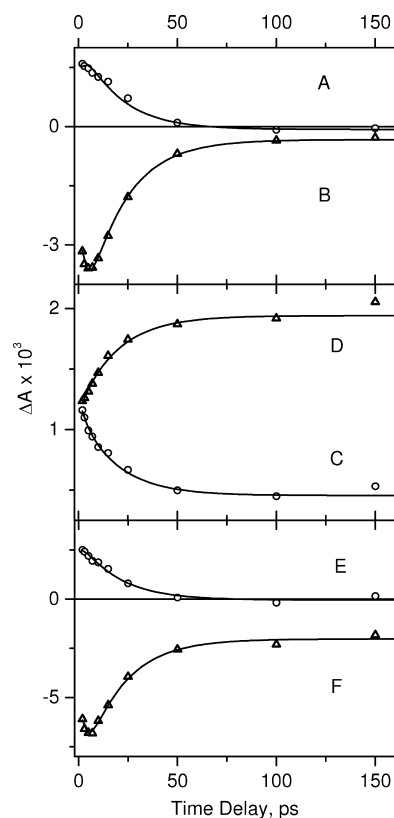


Figure 10. Decay traces obtained in time-resolved infrared experiments for Pt(phen-NDI)Cl₂ in CH₂Cl₂, following excitation with 395 nm, 150 fs laser pulse. Markers represent experimental data points. Solid lines represent fit to the data with the parameters obtained from global fit analysis: two lifetimes τ₁ = 3.0 ± 0.6 ps and τ₂ = 19.3 ± 1.0 ps, and a constant term. Labels A–F on the panels correspond to the band positions indicated in Figure 9.

decrease in the bond order because of a population of an antibonding π* orbital.

Picosecond Time-Resolved IR Data. The ps time-resolved IR (TRIR) experiments were performed in the range 1500–1685 cm⁻¹ with 395 nm (ca. 6 nm fwhm), ~150 fs excitation of solution of **1** in CH₂Cl₂.

Excitation of dichloromethane solutions of **1** results in bleaching of the ground-state absorbancies of ν(CC) at 1583 and of ν(CO) at 1670 cm⁻¹, labeled B and F on Figure 9. The bleaching is accompanied by an instantaneous formation of several transient bands across the spectral range investigated, the most pronounced being at 1576 (A), 1599 (C), 1607 (D), 1647 (G), and 1660 (E) cm⁻¹ (Figure 9). The transient spectrum detected at 2 ps after the laser pulse does not decay uniformly, indicating a presence of several excited states on the picosecond time scale, and, intriguingly, the bleach of the ground-state absorbancies increases with time prior to its recovery.

A set of representative kinetic traces which illustrate the spectral evolution on the picosecond time scale is shown in Figure 10. The capital letters on the upper panel of Figure 9 label the spectral positions corresponding to the kinetics displayed in Figure 10. The kinetic data were analyzed by the global fitting procedure assuming two mono-exponential decay processes and one long-lived component which remains constant on the picosecond time scale. This was the

minimum combination of processes which would allow for a consistent fit of the data. The lifetimes yielded by the global fitting for TRIR spectral evolution are $\tau_1 = 3.0 \pm 0.6$ ps and $\tau_2 = 19.3 \pm 1.0$ ps.

The bleach of the ground state (1583 and 1670 cm⁻¹, kinetics B and F, respectively, on Figure 10) first *increases* in magnitude, indicating further depopulation of the NDI ground state in a process with the 3 ps lifetime. This initial increase is followed by a recovery with the lifetime of 19 ps; however, the parent bleach does not recover completely on the picosecond time scale but reaches a constant magnitude by about 100 ps after which it remains unchanged up to 2 ns. The global fitting procedure yielded some weak but detectable contribution of a 3 ps rise in the transient bands at about 1576 and 1660 cm⁻¹ (kinetics A and E, respectively, on Figure 10), which was followed by a decay with ~ 19 ps lifetime. For the transient bands at about 1599 and 1607 cm⁻¹ (kinetics C and D, respectively, on Figure 10) only the 19 ps component was detected. As shown on Figure 10, the two kinetics, C and D, are complementing each other, one showing a decay (1599 cm⁻¹) while the other showing a rise of a similar magnitude.

Some spectral dynamics associated with the 19 ps lifetime also appears in the range from 1610 to 1647 cm⁻¹, accompanied by a narrowing of the 1647 cm⁻¹ band until it reaches a fwhm of ~ 8 cm⁻¹. A broadband centered at around 1625 cm⁻¹ is also noted.

The spectral evolution of the TRIR data was completed in about 100–150 ps, yielding a spectrum of profile identical to that for the 500 ps delay shown on Figure 9 (-o-), which remained constant up to equipment-limited time delay of 2 ns. On the basis of the results of picosecond transient absorption and microsecond flash photolysis (vide supra), the long-lived transients with maxima at 1607 and 1647 cm⁻¹ were assigned to the ³NDI T₁ excited state.

The difference in the set of lifetimes obtained in the TA experiments (0.9 and 3 ps) and in the TRIR experiments (3 and 19 ps) is noteworthy. It should be noted that the earliest time delay reliably measured in these particular TRIR experiments was 2 ps because of a contribution from experimental artifacts at the early times after the photoexcitation. Hence, the 0.9 ps component observed in picosecond transient absorption experiments could not be observed in the TRIR data. The 3 ps component determined in TRIR experiments matches well within experimental error the 3.5 ps component detected in the TA measurements. Paradoxically, a ~ 19 ps decay process which dominates the temporal evolution of TRIR data was not detected in the picosecond transient absorption experiments.

The origin of 0.9, 3, and 19 ps components observed in the TA and TRIR data and the nature of the corresponding excited states are analyzed below.

Discussion

Picosecond transient absorption, picosecond TRIR, and nanosecond flash photolysis data obtained for **1** indicate a presence of three fast processes, with about 0.9, 3, and 19 ps lifetimes, and of one slow process with 520 μ s lifetime.

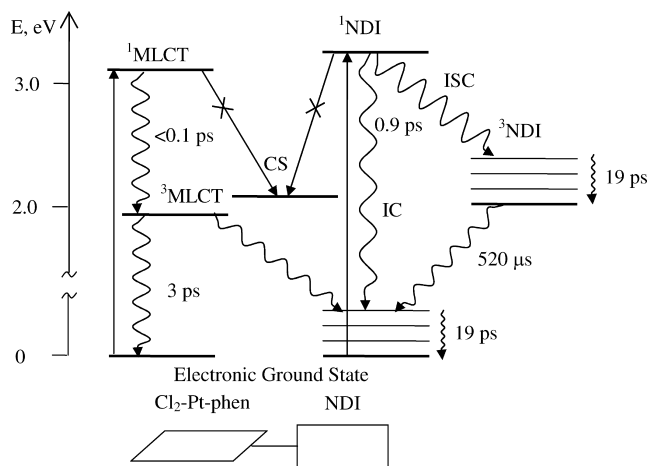


Figure 11. Photophysical diagram for Pt(phen-NDI)Cl₂ in CH₂Cl₂ at r.t. Please see text for the estimated energy level values; CS - charge-separated state, [Pt^{III}(phen-NDI^{-•})Cl₂].

The following excited states can be potentially formed in **1** by photoexcitation: (vibrationally hot) ¹NDI*, vibrationally hot ³NDI, vibrationally relaxed ³NDI; vibrationally hot ³MLCT [Cl₂-Pt^{III}-phen^{-•}-NDI], vibrationally relaxed ³MLCT, vibrationally hot ground state, and a charge-separated state, [Cl₂-Pt^{III}-phen-NDI^{-•}].

The presence of the charge-separated state, [Cl₂-Pt^{III}-phen-NDI^{-•}], would be signaled by an appearance of characteristic absorbancies of NDI^{-•} in either TA^{2,3,15,24} and/or TRIR spectrum. None of the individual transient absorption spectra recorded on the picosecond or nanosecond time scales resemble that of NDI^{-•} which has a very sharp, intense peak at 470 nm and a second intense band at about 600 nm as shown by UV/vis spectroelectrochemistry of **1** (Figure 3). Likewise, IR spectroelectrochemistry shows that NDI^{-•} in **1** has characteristic IR absorbancies at 1514, 1592, and 1629 cm⁻¹ (Figure 8). None of those bands are observed in the TRIR spectra of **1** at any time delay. Therefore, we conclude that charge-separated excited state, [Cl₂-Pt^{III}-phen-NDI^{-•}], is not detected in our system and proceed to the discussion of NDI-localized and MLCT excited states.

The photophysical diagram (Figure 11) summarizes all the experimental findings of the present work and their interpretation. The following thermodynamic parameters were taken into consideration: energy of ¹NDI* 3.22 eV, ³NDI 2.05 eV (averaged from different literature sources),^{3,7,36,73} Pt→phen¹MLCT 3.14 eV (estimated from r.t. absorption spectrum of Pt(phen)Cl₂ in CH₂Cl₂), Pt→phen³MLCT 1.98 eV (estimated from emission spectrum of Pt(phen)Cl₂ in frozen EtOH:MeOH, 4:1 v/v, glass at 77K, this is the top limit as the energy of ³MLCT in solution is expected to be lower). As follows from the ground-state absorption data (Figure 1), there is only very weak (if any) electronic interaction between the electron accepting NDI and Pt-phen-Cl₂ moieties of **1** in its ground electronic state. Hence, as a “zero-order approximation” we consider that the photoexcitation at 395 nm used in the picosecond experiments populates independently the NDI S₁ state and the Pt→phen

(73) Hayes, R. T.; Wasielewski, M. R.; Gosztoła, D. *J. Am. Chem. Soc.* **2000**, *122*, 5563–5567.

¹MLCT state. The energy of the charge-separated state [Cl₂-Pt^{III}-phen-NDI⁻] estimated as the difference between the first oxidation (>1.12 V which was solvent breakdown, Supporting Information, Figure SI 1) and the first reduction (-0.94 V, NDI/NDI⁻) potentials in CH₂Cl₂ would be at least 2.06 eV, which places this state significantly lower in energy than the ¹MLCT state but somewhat higher than the ³MLCT state. In principle, a charge-separated state could be populated from the ¹MLCT state as a result of a thermal electron transfer from phen⁻ formed in the ¹MLCT state of Pt(phen-NDI)Cl₂ to a stronger accepting NDI group. Lack of observation of a charge-separated state indicates that this process in Pt(phen-NDI)Cl₂ can not compete with the ultrafast ISC in ¹MLCT with the formation of the ³MLCT state.^{61–63}

Excited State with 0.9 ps Lifetime, ¹NDI*. The difference spectra of individual excited states (Supporting Information, Figure SI 4) were calculated from the experimental data in the framework of the diagram shown on Figure 11 based on the results of global fitting. The transient spectrum which decays with 0.9 ps lifetime is characterized by a maximum at about 470 nm and a sharp decrease in optical density at wavelengths longer than 600 nm. This spectrum is attributed to the ¹NDI* state.⁷⁴ As was noted previously, the lifetime of these species was too short to be detected in the TRIR experiments. The 0.9 ps lifetime is much shorter than reported for *N,N'*-dialkyl-NDI; one possibility is that such ultrafast decay is due to the presence of a heavy atom. On the other hand, it has also been reported that a variation of the *N*-substituents can dramatically alter the lifetime of the singlet excited states of the imides.^{52,75} Similar ultrafast decay of the singlet state has been reported for the purely organic system, *N*-phenyl-*N'*-alkyl-1,4,5,8-NDI,⁷⁴ and was attributed to a quenching via intramolecular charge-transfer from the phenyl group to the NDI core, with the formation of the NDI-anion. However, since in case of **1** no transient features attributable to the NDI-anion have been observed at any time delay, the charge-transfer mechanism of deactivation of ¹NDI* seems unlikely.⁷⁶ The same 0.9 ps lifetime was reported for the ISC in the intraligand state, ¹IL(stpy) to ³IL(stpy) in [Re(Cl)(CO)₃(stpy)₂], where stpy = 4-styrylpyridine was directly attached to the metal center.

The decay of ¹NDI* in **1** can occur via two competitive pathways, internal conversion (IC) to give NDI ground state recovery and by intersystem crossing (ISC) to populate ³NDI triplet state.

(74) Ganesan, P.; Baggerman, J.; Zhang, H.; Sudholter, E. J. R.; Zuilhof, H. *J. Phys. Chem. A* **2007**, *111*, 6151–6156.

(75) Wintgens, V.; Valat, P.; Kossanyi, J.; Demeter, A.; Biczok, L.; Berges, T. *New J. Chem.* **1996**, *20*, 1149–1158.

(76) A possibility of an electron transfer from coordinated phenanthroline to NDI can not be completely ruled out on the basis of the electrochemical potentials. In DMF, the first irreversible oxidation process at +0.97 V vs. Fc/Fc⁺ is assigned to Pt^{III/IV}; no further oxidation processes have been detected up to the solvent breakdown at about +1.1 V. The first reduction potential of NDI in **1** is -0.90 V vs Fc/Fc⁺. The estimated energy of zero-zero transition in NDI, E₀₀, is about 3.22 eV (Fig. 11, Discussion). Should the oxidation of phenanthroline occur at potentials less positive than 2.32 V, an electron transfer from phenanthroline to NDI could in principle be possible. However, in that case characteristic absorption features of NDI-anion should have been observed.

Excited State with 3 ps Lifetime, {Pt→phen} ³MLCT. The processes characterized by the 3 ps lifetime in the excited state have been detected in both picosecond TA and picosecond TRIR experiments. The corresponding transient absorption spectrum (Supporting Information, Figure SI 4) features a smooth maximum at about 450–475 nm and a broad absorption extending toward NIR range. These features resemble that of the absorption spectrum of the [Pt(phen⁻)Cl₂] anion recorded by UV/vis spectroelectrochemistry (Supporting Information, Figure SI 2) and of the ³MLCT excited state of Pt(phen)Cl₂, ³[Pt^{III}(phen⁻)Cl₂] (Figure 5). Therefore, on the basis of transient absorption data, the excited state with 3 ps lifetime is assigned as ³MLCT Pt→phen in **1**.

As was noted above, the only spectral features detectable in the 1500–1685 cm⁻¹ window of the TRIR experiment are those originating from NDI-localized vibrations, despite predominant excitation of the ¹MLCT state. Therefore, one would not expect to observe any 3 ps dynamics in the TRIR data. However, the 3 ps lifetime is observed in the initial increase of the ground-state bleach at 1583 and 1670 cm⁻¹ and in a weak but distinct increase in the 1576 and 1660 cm⁻¹ transient bands (kinetics A and E, respectively on Figure 10). An increase in the bleach of the ground-state bands indicates a population of an NDI-based state from ³MLCT. It is also logical to assume that the same process adds to the population of the excited state with transient IR features at 1576 and 1660 cm⁻¹, which then decay with the 19 ps lifetime. Interestingly, the same ~3.5 ps lifetime was reported for a ³MLCT - ³IL process in fac-[Re(trans-stpy)(CO)₃(bpy)]⁺.⁶⁰ It should also be noted that because of very short lifetime, the decay processes of ³MLCT are likely to involve a vibrationally hot ³MLCT state.

Gaussian deconvolution of the ground-state electronic absorption spectra of **1** (Figure 1) shows that a 395 (±3 nm) excitation would populate predominantly the ¹MLCT excited state, with only 5–8% of the excitation energy being absorbed by NDI. Nevertheless, only NDI-based features are observed in the TRIR spectra. This could arise for two reasons. First, the IR spectra of the ground state (Supporting Information, Figure SI 3) and DFT calculations show that NDI-based vibrations are much more intense than those localized on the phen fragment in the 1500–1685 cm⁻¹ region. Second, we have shown (see discussion below) that one consequence of the decay of the ³MLCT state is the population of a hot ground state of NDI—the process which occurs with the 3 ps lifetime and is largely finished by the 2 ps time delay when the first reliable TRIR spectrum is recorded. The overall estimate is not unreasonable given that the maximum bleach of NDI ground state detected at 2 ps delay constitutes approximately 5% of the ground-state IR absorbance.

Vibrationally Hot Electronic States with ~19 ps Lifetime. A process with a 19 ps lifetime dominates the temporal evolution of the TRIR spectra but is not observed by transient absorption, suggesting that this process is not related to electronic transitions but is related to a

redistribution of vibrational energy. A likely assignment of such behavior is to vibrationally unrelaxed, “hot” electronic states.

This explanation is consistent with a ~ 0.9 ps lifetime of ¹NDI* excited state formed primarily upon excitation which is proposed to decay to the ground state and to the ³NDI excited state. A fast decay of ¹NDI* on picosecond time scale should lead to vibrationally “hot” product states, especially considering that the energy to be dissipated within such a short time is 3.22 eV for the formation of the ground state and 1.17 eV for the formation of ³NDI. The transient bands A (1576 cm⁻¹) and E (1660 cm⁻¹) are shifted to lower energies from the corresponding ground-state bleaches (B and F, Figure 9) by less than 10 cm⁻¹, which is also characteristic of IR absorbancies originating from excited vibrational levels. Therefore, the 1576 and 1660 cm⁻¹ transient IR bands are assigned to the vibrationally hot ground state. The lifetime of these transients matches the lifetime of the partial parent bleach recovery (19 ps) and lies within the previously reported values for vibrational relaxation in a solvent bath.⁷⁷ It is noteworthy that, at early time delays, the ground-state bleaches are shifted slightly to the higher frequencies if compared to the FTIR spectrum of the ground state (Figure 9) perhaps because of an overlap with the transient bands and that their return to the same position as in the FTIR spectrum occurs with ~ 19 ps lifetime.

The IR bands attributed to ³NDI (1607 cm⁻¹, D, and 1647 cm⁻¹, G) initially appear rather broad and evolve in time. The IR shoulder at about 1600 cm⁻¹ (C) decays with the lifetime of 19 ps with which the 1607 cm⁻¹ band (D) acquires additional intensity. Similar dynamics are observed for the 1610–1650 cm⁻¹ region, in which an initially formed broad vibrational manifold disappears and a distinct band at 1647 cm⁻¹ emerges with about 19 ps lifetime. It should be noted that vibrational relaxation of “hot” ground and “hot” triplet states of NDI in **1** have the same lifetime (ca. 19 ps) within our experimental error.

A formation of the hot ground state of NDI also explains the 3 ps component observed in the initial increase of the parent bleach of $\nu(\text{CO})$ and of the initial grow-in of the transient bands at 1576 and 1660 cm⁻¹. These observations are attributed to a population of the hot ground state of NDI as a result of the decay of the ³MLCT excited state which has 3 ps lifetime. One possible mechanism is that decay of the ³MLCT state is accompanied by vibrational excitation of phenanthroline-based modes, which then relax by intermolecular energy redistribution to the surrounding, including the covalently attached NDI group. A lack of a 3 ps component in the dynamics of the IR bands attributed to ³NDI indicates that ³MLCT state populates NDI in its ground state, but not ³NDI, and is consistent with the slightly lower energy of ³MLCT compared to that of ³NDI (Figure 11).

Excited State with 520 μs Lifetime, ³NDI, and the Corresponding TRIR Spectrum. As discussed above, the transient absorption spectra obtained in flash photolysis experiments (Figure 7) match those reported for ³NDI. Thus, the longest-

lived excited state in **1** is assigned to ³NDI, which possesses a $520 \pm 50 \mu\text{s}$ lifetime in fluid solution at room temperature. This state is formed from the ¹NDI* excited state that was populated initially. Within the range from 1500 to 1680 cm⁻¹ which was studied in this work, the IR absorbancies corresponding to ³NDI are located at 1607 and 1647 cm⁻¹.

To determine the nature of the vibrations observed in the TRIR spectra, DFT calculations were performed in CH₂Cl₂. As was mentioned above, DFT calculations (Supporting Information, Tables S11 and S12) after applying a standard scaling factor of 0.98 predict for the singlet state of *N,N'*-diethyl-NDI in CH₂Cl₂ two $\nu(\text{CO})$ frequencies at 1708 and 1682 cm⁻¹ and a band at 1581 cm⁻¹ of largely $\nu(\text{CC})$ intra-NDI character. Those values match the experimentally recorded frequencies at 1705, 1688, and 1583 cm⁻¹. Calculations performed for the triplet state of the model molecule predict a considerable downward shift of those frequencies, to 1640, 1597, and 1502 cm⁻¹, respectively, after applying the same 0.98 scaling factor.

DFT calculations were also performed on *N*-ethyl-*N'*-(1,10-phenanthroline)-1,4,5,8-naphthalene-diimide which serves as a model of the phen-NDI ligand, in which instead of an octyl group an ethyl group was used. The full vibrational spectrum and the geometries of the singlet ground state and lowest triplet state are given in Supporting Information, Table S13 and S14, and on Figure SI 5. For the singlet ground state of *N*-ethyl-*N'*-(1,10-phenanthroline)-1,4,5,8-naphthalene-diimide the calculations after applying 0.98 scaling factor predict vibrations at 1726 (sh), 1712, 1690, and 1670 cm⁻¹ which are due to different combinations of $\nu(\text{CO})$ and a band of an approximately 50% intensity at 1580 cm⁻¹ which is due to the ring stretching vibration $\nu(\text{CC})$ of the aromatic rings of the NDI. These numbers match well the experimentally detected ones (Table 2), as is also shown in Supporting Information, Figure SI 3. The phenanthroline-based vibrations at 1619, 1595, and 1556 cm⁻¹ (after applying 0.98 scaling factor) are very weak compared to the NDI-based vibrations. This observation supports our conclusion that only NDI-based vibrations are followed in the TRIR experiments in the 1500–1680 cm⁻¹ window.

In the triplet state of *N*-ethyl-*N'*-(1,10-phenanthroline)-1,4,5,8-naphthalene-diimide the NDI-based vibrations are shifted considerably to the lower frequencies. After applying 0.98 scaling factor, the predicted vibrations appear at 1643, 1658 (weak sh), 1613, and 1595 cm⁻¹ (combinations of $\nu(\text{CO})$) and at 1501 cm⁻¹ ($\nu(\text{CC})$ of the aromatic rings of NDI). Importantly, the highest energy $\nu(\text{CO})$ band in the triplet state, 1643 cm⁻¹, is lower in energy than the lowest $\nu(\text{CO})$ in the singlet ground state, 1670 cm⁻¹. These values match the experimentally observed at long time delays bands at 1647 and 1607 cm⁻¹, respectively, and the 1613 cm⁻¹ band appears as a broadband in the TRIR spectra at long time delays. The $\nu(\text{CC})$ band at 1501 cm⁻¹ would be just outside the experimental window in our TRIR experiments. The very weak bands due to phenanthroline moiety appear largely unchanged.

It therefore follows that the bands at 1647 and 1607 cm⁻¹ observed in the TRIR spectrum of the [Pt(phen-³NDI)Cl₂]* are due to $\nu(\text{CO})$ of the NDI fragment in its triplet state.

(77) Elsaesser, T.; Kaiser, W. *Annu. Rev. Phys. Chem.* **1991**, *42*, 83–107.

This assignment is consistent with a large shift toward lower frequencies upon promotion into the triplet excited state reported for a similar chromophore, PNI (4-piperidinyl-1,8-naphthalimide), attached to a phenanthroline ligand in Ru^{II} complexes.⁴⁸ The ground-state symmetric and antisymmetric $\nu(\text{CO})$ stretch of PNI, at 1705 and 1668 cm^{-1} , respectively, were shifted to 1643 and 1567/1597 cm^{-1} in its ³PNI state (the latter appearing as a double band due to interference of the ground-state band located at 1585 cm^{-1} , which the authors preliminary assigned as predominantly $\nu(\text{CH})$). Importantly, no transient IR bands were observed for ³PNI at higher frequencies, up to 1800 cm^{-1} . The authors assigned both transient bands to $\nu(\text{CO})$ and concluded that the 1585 cm^{-1} band shifts to the frequencies below 1500 cm^{-1} .⁴⁸ A considerable downward shift of $\nu(\text{CO})$ vibrations upon promotion to the triplet state was also reported in the TRIR studies of riboflavine tetraacetate (RBTA) and lumiflavine, which contain $\sim\text{C}(\text{O})-\text{N}-(\text{CO})\sim$ fragment.⁷⁸ The 1647 cm^{-1} band observed in the TRIR spectrum of **1** is very close to the 1652 cm^{-1} band reported for ³RBTA, which was assigned to $\nu(\text{CO})$ with an excellent agreement with the DFT calculations.

The assignment of 1607 and 1647 cm^{-1} transient IR bands to $\nu(\text{CO})$ of the ³NDI in **1** implies a considerable shift to lower frequencies upon promotion to the ³NDI state, and a corresponding reduction in the C=O bond order. A negative shift of 63 cm^{-1} and 58 cm^{-1} from the energies of the $\nu(\text{CO})$ in the singlet ground state is estimated for the two most intense $\nu(\text{CO})$ bands, which is close to that previously reported for the shift in $\nu(\text{CO})$ in the PNI chromophore upon promotion to its triplet excited state.

Consistent with the triplet nature of the long-lived excited state, excitation of a 7×10^{-6} M solution of **1** in CH_2Cl_2 with a 355 nm laser pulse leads to a formation of singlet oxygen with the 14 (± 3) % yield. The low yield of ¹O₂ production is consistent with the 10 (± 3)% yield of ³NDI state in **1** determined relative to benzophenone (see Experimental Section for details).

Conclusions

A representative Pt^{II} diimine-imide dyad, Pt(phen-NDI)Cl₂, where NDI = strongly electron accepting 1,4,5,8-naphthalenediimide group, has been synthesized and fully characterized. UV/vis/IR spectroelectrochemistry and EPR studies of electrochemically generated anions confirmed that the LUMO in this system is localized on the NDI acceptor group. The lowest allowed electronic transition in Pt(phen-NDI)Cl₂ is charge-transfer to-diimine of a largely Pt \rightarrow phen MLCT character. This transition has virtually the same energy and extinction coefficient as that in Pt(phen)Cl₂, indicating little electronic communication between the {NDI} and the {Cl₂Ptphen} parts of the molecule **1** in its ground electronic state.

The lowest excited state of the model compound Pt(phen)Cl₂, assigned as ³MLCT, possesses an absorption spectrum which has two broad maxima at 450 and 580 nm

and the lifetime of 1.7 ± 0.5 ps. These data were used to pinpoint the formation of ³MLCT Pt \rightarrow phen excited state in Pt(phen-NDI)Cl₂.

The presence of intense $\nu(\text{CO})$ and ring vibrations in the NDI fragment enabled the use of time-resolved infrared spectroscopy to follow the redistribution of electron density in Pt(phen-NDI)Cl₂ after initial photoexcitation and to determine the role of vibrationally hot electronic states. A combination of picosecond time-resolved infrared spectroscopy, picosecond transient absorption, and nanosecond flash photolysis methods were used to elucidate the excited-state dynamics of Pt(phen-NDI)Cl₂. The processes with the lifetimes of 0.9 ps, 3 ps, 19 ps, and 520 μs were identified and summarized in Figure 11.

Excitation of **1** with 395 nm femtosecond laser pulses populates independently the ¹MLCT and the ¹NDI* excited states. The ¹MLCT state then undergoes an ultrafast intersystem crossing into the ³MLCT state. The predominant decay pathway of the ³MLCT is a back electron transfer process with ~ 3 ps lifetime, which leads to the restoration of the ground state. Picosecond TRIR experiments revealed that a decay of the ³MLCT state partially populates a vibrationally hot ground state of the NDI fragment, perhaps via intramolecular energy redistribution. A thermodynamically possible decay pathway of the initially populated ¹MLCT to the charge-separated, charge-transfer-to-NDI excited state, [Pt^{III}(phen-NDI⁻)Cl₂], is not observed. This finding could be explained by an ultrafast intersystem crossing of ¹MLCT to ³MLCT state which lies at least 0.08 eV lower in energy than [Pt^{III}(phen-NDI⁻)Cl₂]. A possibility of the inversion of the relative energies of those states in **1** by solvent polarity is presently under investigation.

The ¹NDI* state in **1** has about 0.9 ps lifetime and decays to form a vibrationally hot NDI ground state as well as a vibrationally hot ³NDI. The lifetime of vibrational relaxation of the NDI-localized vibrations in both ground and ³NDI electronic states is ~ 19 ps.

The longest-lived excited state in Pt(phen-NDI)Cl₂ generated under 355–395 nm excitation is ³NDI, [Pt(phen-³NDI)Cl₂]*, which has the lifetime of 520 μs —remarkably long for a Pt^{II} complex in fluid solution at room temperature. The IR signature of this state includes the $\nu(\text{CO})$ bands at 1607 and 1647 cm^{-1} which are shifted considerably to lower energies, by 63 and 58 cm^{-1} , respectively, if compared to their ground-state counterparts.

Pt(phen-NDI)Cl₂ acts as a modest photosensitizer of singlet oxygen, a property which, taken in conjunction with the well-established intercalating properties of NDI, is of potential biological relevance.

Experimental Section

Syntheses. Synthesis of 5-Amino-1,10-phenanthroline (phen-NH₂). Hydrazine monohydrate (1 mL, excess) was added to a suspension of 5-nitro-1,10-phenanthroline (250 mg, 1.11 mmol) and Pd/C (10% Pd, 25 mg, catalyst) in degassed ethanol (15 mL) under N₂. The reaction mixture was sonicated for 1 h at room temperature, refluxed for 24 h, cooled to r.t., filtered to remove Pd/C, evaporated to dryness, and dried under vacuum to yield product as a yellow

(78) Martin, C. B.; Shi, X. F.; Tsao, M. L.; Karweik, D.; Brooke, J.; Hadad, C. M.; Platz, M. S. *J. Phys. Chem. B* **2002**, *106*, 10263–10271.

solid in >95% yield (C₁₂H₉N₃, M.W. 195.22). In some cases crude product showed the presence of hydrazine by ¹H NMR. In this case, the product was redissolved in 100 mL of CHCl₃ and washed with 3 × 100 mL of H₂O. The organic layer was dried with MgSO₄, filtered and the solvent removed. ¹H NMR (DMSO-*d*₆): 6.10–6.17 (m, br, 2H), 6.85 (s, 1H), 7.50 (dd, *J* 8.0, 4.3, 1H), 7.73 (dd, *J* 8.3, 4.3, 1H), 8.03 (dd, *J* 8.3, 1.5, 1H), 8.63–8.70 (m, 2H), 9.04 (dd, *J* 4.3, 1.5, 1H).

N-octyl-1,4,5,8-naphthalenetetracarboxylic monoanhydride³⁵ and *N,N'*-dioctyl-1,4,5,8-naphthalenediimide²⁴ were prepared as described previously.

Synthesis of Phen-NDI. phen-NH₂ (216 mg, 1.11 mmol) and *N*-octyl-1,4,5,8-naphthalenetetracarboxylic monoanhydride (421 mg, 1.11 mmol) were stirred in dry degassed DMF (4 mL) at 140 °C for 24 h. Cooling to r.t. and addition of ethanol (20 mL) precipitated the crude product. It was filtered, washed with ethanol and ether, and purified by column chromatography (17 g of silica, 0.2–1.0% CH₃OH in CH₂Cl₂) to give 361 mg (0.61 mmol, 55%) of cream product. Calcd for C₃₄H₂₈N₄O₄·(H₂O)₂ (M.W. 592.64): C, 68.91; H, 5.44; N, 9.45. Found: C, 69.22; H, 5.14; N, 9.40. EI MS *m/z*: 556 (100%, M⁺). ¹H NMR (CDCl₃): 0.84–0.92 (m, br, 3H), 1.22–1.55 (m, br, 10H), 1.70–1.85 (m, br, 2H), 4.19–4.27 (m, br, 2H), 7.60 (dd, *J* 8.6, 4.6, 1H), 7.72 (dd, *J* 8.3, 4.6, 1H), 7.90 (s, 1H), 8.00 (dd, *J* 8.3, 1.8, 1H), 8.31 (dd, *J* 8.3, 1.5, 1H), 8.86 (s, 4H), 9.25 (dd, *J* 4.3, 1.5, 1H), 9.30 (dd, *J* 4.6, 1.8, 1H).

Synthesis of Pt(phen-NDI)Cl₂. PtCl₂(DMSO)₂ (150 mg, 0.36 mmol) and phen-NDI (213 mg, 0.36 mmol) were stirred in degassed ethanol (15 mL) at 78 °C for 24 h under N₂ to give a yellow precipitate of the product. The reaction mixture was cooled to r.t. and filtered. The product was washed with methanol and ether and purified by column chromatography (15 g of silica, 0.5–0.75% CH₃OH in CH₂Cl₂, major yellow band collected) to give 191 mg (0.23 mmol, 64%) of bright yellow or orange product. The complex is soluble in CH₂Cl₂ and acetone. Calcd for C₃₄H₂₈Cl₂N₄O₄Pt (M.W. 822.59): C, 49.64; H, 3.43; N, 6.81. Found: C, 48.67; H, 3.27; N, 6.59. ¹H NMR (CDCl₃): 0.83–0.93 (m, br, 3H), 1.23–1.53 (m, br, 10H), 1.65–1.85 (br, 2H), 4.17–4.29 (t, br, 2H), 7.82–7.92 (dd, 1H), 7.95–8.05 (dd, 1H), 8.16 (s, 1H), 8.32–8.39 (dd, 1H), 8.67–8.75 (dd, 1H), 8.87 (s, 4H), 10.06–10.15 (m, 2H).

Spectroscopic and Electrochemical Studies. In-house facilities were used for CHN and EI MS analysis. The following instruments were used: absorption spectra, a Cary 50 Bio UV–visible spectrophotometer; ¹H NMR spectra (presented as δ in ppm and *J* in Hz), a Bruker 250 MHz spectrometer.

Ground state FTIR data were obtained on N₂-purged Spectrum One FTIR spectrometer (Perkin-Elmer).

EPR spectra were recorded on a Bruker EMX spectrometer, and spectral simulations were accomplished using WINEPR SimFonia v1.25 software. The concentration of the samples for EPR studies obtained by bulk electrolysis was 1 mM.

Electrochemistry. Standard cyclic and square-wave voltammetric and coulometric studies were carried out using an Autolab PGSTAT20 potentiostat. The voltammetry was carried out under an atmosphere of argon using a three-electrode arrangement in a single compartment cell. A glassy carbon working electrode, a Pt wire secondary electrode, and a saturated calomel reference electrode, chemically isolated from the test solution via a bridge tube containing electrolyte solution and fitted with a porous vycor frit, were used in the cell. The solutions were 10⁻³ M in the test compound unless stated otherwise; [NBu₄][BF₄] (0.4 M for CH₂Cl₂ and 0.2 M for DMF) was used as supporting electrolyte. The redox potentials are quoted versus the ferrocenium-ferrocene couple. Coulometric studies, at a controlled potential, were carried out using

a two-compartment cell. The Pt/Rh gauze basket working electrode was separated from the wound Pt/Rh gauze secondary electrode by a glass frit. A saturated calomel reference electrode was bridged to the test solution through a vycor frit orientated at the center of the working electrode. The working electrode compartment was fitted with a magnetic stirrer bar, and the test solution was stirred rapidly during electrolysis. The UV/vis spectroelectrochemical experiments were carried out on about 0.5 mM solutions in optically transparent electrochemical (OTE) cell (modified quartz cuvette, with 0.5 mm optical path length). The cell comprised a three-electrode configuration, consisting of a Pt/Rh gauze working electrode, a Pt wire secondary electrode (in a fritted PTFE sleeve), and a saturated calomel electrode, chemically isolated from the test solution via a bridge tube containing electrolyte solution and terminated in a porous frit. The potential at the working electrode was controlled by a Sycopel Scientific Ltd. DD10 M potentiostat. The (spectro)electrochemical UV/vis data were recorded on a Perkin-Elmer Lambda 16 spectrophotometer. The cavity was purged with dinitrogen, and temperature control at the sample was achieved by flowing cooled dinitrogen across the surface of the cell.

Picosecond Transient Absorption. Experiments were performed at the B.I. Stepanov Institute of Physics, Minsk, on a pump–probe spectrometer based on a homemade original fs Ti:Sapph pulsed oscillator and regenerative amplifier system operated at 10 Hz repetition rate.⁷⁹ The Ti:Sapph master oscillator was synchronously pumped with the doubled output of a homemade mode-locked picosecond pulsed Nd:YAG laser. The regenerative amplifier was pumped with a ns Q-switched Nd:YAG laser LS-2134 (LOTIS TII). The pulse width and energy of the Ti:Sapph system after the amplifier were about 150 fs and 0.5 mJ, respectively, tuneable over the spectral range 760–820 nm. The fundamental output of the Ti:Sapph system (790 nm output wavelength was set for present study) was split into two beams in the ratio 1:4. The more intense beam was passed through a controlled delay line and after frequency doubling (to provide 395 nm radiation) was utilized for sample pumping. The energy of the 395 nm pump pulses was about 40 μ J, being focused to a 500 × 500 μ m spot on the sample. The second beam of the fundamental frequency was used for the generation of a femtosecond supercontinuum (by focusing into 1 cm path length cell with water), which served as the probe radiation. The continuum probe light was split with a beam splitter into two pulses (reference and signal), identical in intensity, and the signal was focused on the sample by mirror optics. The spectra of both pulses were recorded for each laser flash by a polychromator equipped with a CCD camera and transferred to the computer. The time resolution of the setup is limited by the pump and probe pulse duration and estimated as about 0.2 ps. A solution of **1** in CH₂Cl₂ in a 5 mm quartz cell was bubbled with Ar prior to the experiments, and a positive pressure of the inert gas was maintained over the course of the experiment.

Picosecond Time-Resolved IR. Studies were performed in the Ultrafast Spectroscopy Laboratory, Rutherford Appleton Laboratory, STFC, U.K., on the setup which was described in detail elsewhere.⁸⁰ The estimate of the time resolution of the TRIR setup is about 0.4 ps for these experiments. Briefly, part of the output from a 1 kHz, 790 nm, 150 fs, 1 mJ Ti:Sapphire oscillator/regenerative amplifier was used to pump a white light continuum seeded BBO OPA. The

(79) Blokhin, A. P.; Gelin, M. F.; Buganov, O. V.; Dubovskii, V. A.; Tikhomirov, S. A.; Tolstorozhev, G. B. *J. Appl. Spectrosc.* **2003**, *70*, 70–78.

(80) Towrie, M.; Grills, D. C.; Dyer, J.; Weinstein, J. A.; Matousek, P.; Barton, R.; Bailey, P. D.; Subramaniam, N.; Kwok, W. M.; Ma, C.; Phillips, D.; Parker, A. W.; George, M. W. *J. Appl. Spectrosc.* **2003**, *57*, 367–380.

signal and idler produced by this OPA were difference frequency mixed in a type I AgGaS₂ crystal to generate tuneable mid-infrared pulses (ca. 150 cm⁻¹ fwhm, 0.1 μJ). Second harmonic generation of the residual 790 nm light provided 395 nm pulses, which were used to excite the sample (typical excitation energy 3 μJ, focus 150 × 150 μm, the energy density was thus approximately the same as in the transient absorption measurements). All measurements were carried out at the magic angle polarization. Changes in infrared absorption were recorded by normalizing the outputs from a pair of 64-element HgCdTe linear array detectors on a shot-by-shot basis. A solution of **1** in CH₂Cl₂ was bubbled with dinitrogen prior to the experiments, and positive pressure of the inert gas was maintained over the course of the experiment. Measurements were performed in 100–500 μm IR cells mounted on a 2D-translational stage which was raster-scanned in the *x* and *y* directions during irradiation. The FTIR spectra recorded before and after the TRIR experiments confirm the absence of the photodegradation (Supporting Information, Figure SI 6).

Nanosecond Flash Photolysis. Studies were conducted in Sheffield on the home-built setup. The Q-switched Nd:YAG laser LS-2137U (LOTIS TII) tripled output (7 ns, 355 nm, pulse energy attenuated down to 0.5 mJ to avoid triplet–triplet annihilation) was used as the excitation source, while the probing was performed with a steady-state 150W Hamamatsu Arc Xe lamp. The probe beam was detected by a monochromator equipped with a home-built detector unit, based on FEU-118 PMT. Detector current output was coupled into a Tektronix TDS 3032B digital oscilloscope and subsequently transferred to the computer. The instrumental response function is estimated as about 22 ns fwhm. Solutions of **1** in CH₂Cl₂ were degassed by the freeze–pump–thaw technique in 10 mm quartz cells and subsequently saturated with argon.

Singlet Oxygen Generation was investigated as described in detail elsewhere.⁸¹

Determination of the Triplet Quantum Yield. The triplet yield was determined by a comparative technique⁸² using benzophenone in benzene as a standard ($\Phi_T = 1.0$, $\epsilon_{T-T} = 7220 \text{ M}^{-1} \text{ cm}^{-1}$ at 530 nm⁸³). The solvents employed were distilled CH₂Cl₂ for Pt(phen-NDI)Cl₂ and benzene (Merk, Uvasol for spectroscopy, ≥99.8%) for benzophenone. The concentrations used were $5 \times 10^{-6} \text{ M}^{-1}$ for Pt(phen-NDI)Cl₂ in CH₂Cl₂ and $1.2 \times 10^{-3} \text{ M}^{-1}$ for benzophenone in benzene. The measurements were performed at a number of excitation energy values in the range 0.82–4.6 mJ, the signal dependence on energy was linear in this range, and the ground-state depletion was satisfactorily low under such conditions. The triplet–triplet absorption was monitored in the maxima of the corresponding T-T absorption spectra, at 490 nm for Pt(phen-NDI)Cl₂, and at 530 nm for benzophenone. Both compounds have negligible ground-state absorbance at these wavelengths. Under the conditions of equal ground-state absorption at excitation wavelength, and under identical excitation conditions, the sample triplet quantum yield $\Phi_{T\text{SAMPLE}}$ can be calculated as

$$\Phi_{T\text{SAMPLE}} = \Phi_{T\text{STANDARD}} \frac{\Delta A_0^{\text{SAMPLE}} \epsilon_{T-T}^{\text{STANDARD}}}{\Delta A_0^{\text{STANDARD}} \epsilon_{T-T}^{\text{SAMPLE}}} \quad (1)$$

where $\Phi_{T\text{STANDARD}}$ is the standard triplet state formation quantum yield, ΔA_0 is the amplitude of triplet–triplet absorption at zero delay time at the wavelength corresponding to the triplet–triplet extinction coefficient value, ϵ_{T-T} is the extinction coefficient for triplet–triplet absorption.

For Pt(phen-NDI)Cl₂ in CH₂Cl₂, the value of the extinction coefficient, ϵ_{T-T} , in the maximum of triplet–triplet absorption at 490 nm was assumed to be $11625 \text{ M}^{-1} \text{ cm}^{-1}$, as reported previously for naphthalene diimide derivatives at 485 nm.^{2,7}

The yield of ³NDI state in Pt(phen-NDI)Cl₂ in CH₂Cl₂ determined in this way was 10(±3)%.

The analysis of time-resolved data to obtain decay lifetimes was performed using Igor Pro software (WaveMetrics, Inc.). The decay kinetics were fitted to the sum of exponentials (with an addition of a long-lived component if needed) using a least-squares algorithm built into Igor Pro. In the case of picosecond transient absorption data, the deconvolution of the instrumental response (approximated as Gaussian profile of several hundred fs fwhm) from experimental decay kinetics was applied. The determination of the actual zero time delay for each spectral position was incorporated in the data analysis algorithm, which automatically provided chirp correction. For picosecond transient absorption and TRIR data, global fitting was applied to analyze simultaneously the decay kinetics obtained for a number of spectral points, which considerably increased reliability of the fitted lifetimes and also provided the individual spectra of decaying species in case of transient absorption data.

Global Fitting. The global fitting of the time-resolved data for **1** was performed assuming a sum of two exponents and a long-lived component. Collectively, as a result of global fitting, two lifetimes were obtained for the whole set of kinetics covering the full spectral span of the transient absorption experiment, and the values of pre-exponential amplitudes (including the amplitude of the long-lived component) were stored for every kinetic trace. The full spectrum for exponential decays as well as the long-lived component (amplitude vs wavelength) was obtained in this way. Once this procedure was performed, the difference absorption spectra of the excited states contributing to the sample's temporal evolution could be obtained easily for the dynamic energy-level model as the one shown on Figure 11. The global fitting procedure could be performed directly for any particular kinetic model under consideration, but we did global fitting for the simple sum of exponentials as it is easy to recalculate the component spectra between different models (i.e., independent decays, subsequent decays, one component decaying back to the ground state while another forming long-lived state, etc.).

Calculations. Vibrational spectra of the *N,N'*-diethyl-1,4,5,8-naphthalene-diimide and *N*-octyl-*N'*-(1,10-phenanthroline)-1,4,5,8-naphthalene-diimide, were calculated for the singlet state and for the lowest triplet state. These molecules serve as models for the NDI (Scheme 1) and phen-NDI ligand, in which octyl groups are replaced by ethyl groups to reduce computational time. A very good agreement with the experimental data was obtained. All calculations were performed using the SMP version of the Gaussian 03 program package⁸⁴ with the B3LYP functional method.⁸⁵ Gaussian 03 package was compiled using the Intel ifc compiler version 7.1 with ATLAS version 3.6.0⁸⁶ and the GOTO implementation of BLAS.⁸⁷ In all calculations we used the 6–311G(d,p) basis set.^{88,89} As a result, the calculations contained 516 basis functions and 168 electrons for the *N,N'*-diethyl-1,4,5,8-naphthalene-diimide and 744 basis functions and 244 electrons for *N*-octyl-*N'*-(1,10-phenanthroline)-1,4,5,8-naphthalene-diimide. No symmetry was taken into account in our calculations.

In all calculations the following procedure was adopted. We optimized the structures for both singlet state and triplet state

(81) Shavaleev, N. M.; Adams, H.; Best, J.; Edge, R.; Navaratnam, S.; Weinstein, J. A. *Inorg. Chem.* **2006**, *45*, 9410–9415.

(82) Amand, B.; Bensasson, R. *Chem. Phys. Letts.* **1975**, *34*, 44–48.

(83) Hurley, J. K.; Sinai, N.; Linschitz, H. *Photochem. Photobiol.* **1983**, *38*, 9–14.

separately, whereby solvent interactions were treated using the Polarizable Continuum Model (PCM)^{90,91} and the United Atom Topological Model⁹² applied to radii optimized at the Hartree–Fock 6–31(d) level of theory. This set of radii was used to retain compatibility with the implementation of PCM in earlier versions of Gaussian 03. As was said above, for computational efficiency, we pared down the molecules investigated to contain an ethyl group instead of an octyl group attached to the nitrogen atom(s). After obtaining the minimum energy structures, we performed frequency

calculations. In all our calculations, we set the integral accuracy to “Ultrafine” because in our experience this aids in convergence with PCM calculations.

Acknowledgment. We thank the Engineering and Physical Sciences Research Council, U.K. (GR/T03345 and T03352), the Royal Society, U.K., and RFBR, Russia, for funding and Rutherford Appleton Laboratory, Science and Technology Funding Council, U.K. for a loan of the laser and for TRIR beam time. I.V.S. thanks EU for a Marie Curie Incoming International Fellowship (MIIF-CT-2006-040168). We are grateful to CMSD Research Network of CCLRC and EPSRC CAN award for the PhD studentship to J.B. We offer fulsome acknowledgements to Dr N. M. Shavaleev for developing synthetic procedures for this work. We are indebted to Dr. R. Edge and Dr. S. Navaratnam for performing measurements of the yield of singlet oxygen generation.

Supporting Information Available: Figures SI 1 to SI 6 and infrared spectral data for the compounds. This material is available free of charge via the Internet at <http://pubs.acs.org>.

IC801022H

- (84) Frisch, M. J.; Trucks, G. W.; Schlegel, H. B.; Scuseria, G. E.; Robb, M. A.; Cheeseman, J. R.; Montgomery, J. A.; Vreven, K. N. K.; Burant, J. C.; Millam, J. M.; Iyengar, S. S.; Tomasi, J.; Barone, V.; Mennucci, B.; Cossi, M.; Scalmani, G.; Rega, N.; Petersson, G. A.; Nakatsuji, H.; Hada, M.; Ehara, K.; Toyota, R.; Fukuda, J.; Hasegawa, M.; Ishida, T.; Nakajima, Y.; Honda, O.; Kitao, H.; Nakai, M.; Klene, X.; Li, J. E.; Knox, H. P.; Hratchian, J. B.; Cross, V.; Bakken, C.; Adamo, J.; Jaramillo, R.; Gomperts, R. E.; Stratmann, O.; Yazyev, A. J.; Austin, R.; Cammi, R.; Pomelli, C.; Ochterski, J. W.; Ayala, P. Y.; Morokuma, K.; Voth, G. A.; Salvador, P.; Dannenberg, J. J.; Zakrzewski, V. G.; Dapprich, S.; Daniels, A. D.; Strain, M. C.; Farkas, O.; Malick, D. K.; Rabuck, A. D.; Raghavachari, K.; Foresman, J. B.; Ortiz, J. V.; Cui, Q.; Baboul, A. G.; Clifford, S.; Cioslowski, J.; Stefanov, B. B.; Liu, G.; Liashenko, A.; Piskorz, P.; Komaromi, I.; Martin, R. L.; Fox, D. J.; Keith, T.; Al-Laham, M. A.; Peng, C. Y.; Nanayakkara, A.; Challacombe, M.; Gill, P. M. W.; Johnson, B.; Chen, W.; Wong, M. W.; Gonzalez, C.; Pople, J. A. *Gaussian 03*, Revision B.05; Gaussian, Inc.: Wallingford, CT, 2004.
- (85) Becke, A. D. *J. Chem. Phys.* **1993**, *98*, 5648.
- (86) Whaley, R. C.; Petitet, A.; Dongarra, J. J. *Parallel Computing* **2001**, *27*, 3; also available as University of Tennessee LAPACK Working Note #147, UT-CS-100-448, 2000 (www.netlib.org/lapack/lawns/lawn2147.ps).
- (87) See <http://www.cs.texas.edu/users/flame/goto>.
- (88) McLean, A. D.; Chandler, G. S. *J. Chem. Phys.* **1980**, *72*, 5639.
- (89) Krishnan, R.; Binkley, J. S.; Seeger, R.; Pople, J. A. *J. Chem. Phys.* **1980**, *72*, 650.
- (90) Mennucci, B.; Tomassi, J. *J. Chem. Phys.* **1997**, *106*, 5151.
- (91) Cossi, M.; Barone, V.; Mennucci, B.; Tomassi, J. *Chem. Phys. Lett.* **1998**, *286*, 253, and references therein.
- (92) Barone, V.; Cossi, M.; Tomassi, J. *J. Chem. Phys.* **1997**, *107*, 3210.